FTIR, Raman, and UV-Vis spectroscopic and DFT investigations of the structure of iron-lead-tellurate glasses

Simona Rada, Adriana Dehelean, Eugen Culea

FTIR, Raman, UV-VIS spectroscopy and DFT investigations on the structure of the iron-lead-tellurate glasses

Received: 18.06.2010 / **Accepted:** 05.11.2010

Simona Rada[1,✉], Adriana Dehelean[1,2], and Eugen Culea[1]

[1]Department of Physics, Technical University of Cluj-Napoca, 400641, Romania

[2]Nat. Inst. For R&D of Isotopic and Molec. Technologies, Cluj-Napoca, Romania

✉Email: Simona.Rada@phys.utcluj.ro; radasimona@yahoo.com

Abstract

In this paper, we have analyzed the effects of iron ions intercalations on lead-tellurate glasses by investigations of FTIR, Raman and UV-VIS spectroscopy. The homogeneous glass system has compositions $xFe_2O_3 \cdot (100-x)[4TeO_2 \cdot PbO_2]$ where x = 0-60 mol%.

The presented observations in these mechanisms show that the lead ions have an affinity pronounced towards $[TeO_3]$ structural units yielding the deformation of the Te-O-Te linkages and pursuant to the intercalation of $[PbO_n]$ (n=3, 4) and $[FeO_n]$ (n=4, 6) entities in the $[TeO_4]$ chain network. The formation of $[FeO_4]^{-1}$ structural units with negative charge implies the attraction of Pb^{+2} ions for compensation of electrical charge. By increasing of the Fe_2O_3 content up to 60mol%, the accommodation of the network with excess of oxygen can be supported by the formation of $[FeO_6]$ structural units and the conversion of $[TeO_4]$ into $[TeO_3]$ structural units.

For higher Fe_2O_3 content, the Raman spectra revealed a greater degree of depolymerization of vitreous network than do the FTIR spectra. The bands due to the Pb-O bond vibrations are very strongly polarized and the $[TeO_4]$ structural units convert into $[TeO_3]$ units via an intermediate coordination labeled as $[TeO_{3+1}]$ structural units.

Our UV-VIS spectroscopic data show two mechanisms: i) the conversion of the Fe^{+3} to Fe^{+2} species in same time with the oxidation of Pb^{+2} to Pb^{+4} ions for sample with smaller Fe_2O_3 content; ii) when the Fe_2O_3 content is higher ($x \geq 50$ mol%), the Fe^{+2} ions capture positive holes and are transferred to Fe^{+3} ions through photochemical reaction while the Pb^{+2} ions are formed by reduction of the Pb^{+4} ions.

DFT calculations show that the addition of Fe_2O_3 content to lead-tellurate glasses seems to break the axial Te-O bonds and the $[TeO_4]$ structural units are transformed little by little into $[TeO_{3+1}]$ and $[TeO_3]$ type polyhedra. The analysis of these data further indicates a gradual adaptation of lead ions from covalent to ionic environment. Then, there is a change transfer between the tellurium atoms tri- and tetra-coordinated due to the flexibility of the lead-tellurate network to form the appropriate coordination environments with structural units of opposite charge such as iron ions, $[FeO_4]^{-1}$.

Keywords Iron-lead-tellurate glasses · FTIR and UV-VIS spectroscopy · DFT calculations

Introduction

Oxide glasses including transition metal ions were extensively studied due to their semiconducting properties [1-6]. The conduction in ternary iron oxide glasses was confirmed to be due to hopping conduction of polaron [7].

The structural role of lead oxide in many oxide glasses is unique since lead oxide is known to play a dual role both as a network modifier and former [1, 8, 9]. This role depends on the type of bond between lead and oxide. These studies proposed that at high content of PbO [7, 8], it would become difficult to form a network structure of binary glasses.

The structure and the properties of the oxide glasses are dependent strongly on the nature and the concentration of the constituent oxides. In normal glass system, the modifier atoms cause the network to break. In tellurate glasses, the modifier atoms cause the modification of the basic structural units such as [TeO_4] trigonal bipyramid and [TeO_3] trigonal pyramid with one of the equatorial position occupied by a lone pair of electrons [9].

The objective of this work is to analyze the structural and spectroscopic properties iron-lead-tellurate glasses by investigations of FTIR, Raman, UV-VIS spectroscopy and DFT calculations. Particular attention is devoted to understand the role played by lead and iron ions in the determining the structural properties of the glasses.

Experimental

Glasses were prepared by mixing and melting of appropriate amounts of lead (IV) oxide, tellurium oxide (IV) and iron (III) oxide of high purity (99,99 %, Aldrich Chemical Co.). Reagents were melted at 1000 $^{\circ}$C at 15 minutes and quenched.

The samples were analyzed by means of X-ray diffraction using a XRD-6000 Shimadzu Diffractometer, with a monochromator of graphite for Cu-Kα radiation (λ = 1.54 Å) at room temperature. The X-ray diffraction patterns did not reveal the crystalline phase in the sample with $x \geq 60$ mol% Fe_2O_3.

The FT-IR absorption spectra of the glasses in the 370-1200 cm^{-1} spectral range were obtained with a JASCO FTIR 6200 spectrometer using the standard KBr pellet disc technique. The spectra were carried out with a standard resolution of 2 cm^{-1}.

UV-Visible absorption spectra of the powdered glass samples were recorded at room temperature in the range 250-800 cm^{-1} using a Perkin-Elmer Lambda 45 UV/VIS spectrometer equipped with an integrating sphere. These measurements were made on glass powder dispersed in KBr pellets.

The Raman spectra have been recorded for bulk glasses using an integrated FRA 106 Raman module in a 180° scattering geometry, at room temperature. The spectral resolution was 1cm^{-1}.

The geometry optimization of the proposed structural model was carried out using the density function theory (DFT). The DFT computations were performed with B3PW91/CEP-4G/ECP method using the Gaussian'03 program package [10].

Results and discussion

FTIR spectroscopy

Fig. 1 show the FTIR spectra of the Fe_2O_3 doped lead-tellurate glasses. The examination of the FTIR spectra of the $xFe_2O_3 \cdot (100-x)[4TeO_2 \cdot PbO_2]$ glasses shows that the Fe_2O_3 content modifies the characteristic IR bands as follows:

i) The larger band centered at ~625 cm^{-1} is assigned to the stretching mode of the [TeO_4] trigonal bipyramidal with bridging oxygens. The shoulder located at about 750 cm^{-1} indicates the presence of [TeO_3] structural units, Table 1 [10-15]. For all glasses, the general trend is shift towards higher wavenumber (668 cm^{-1}). This suggests the conversion some [TeO_4] to [TeO_3] structural units because the lead ions have a strong affinity towards these groups containing non-bridging oxygens, which are negative-charged.

ii) The broader band centered at about 670 cm^{-1} can be attributed to Pb-O bonds vibrations from [PbO_3] and [PbO_4] structural units [16-19]. With increasing Fe_2O_3 content up to 15

mol%, the formation of larger numbers of non-bridging oxygen's yields the apparition of [PbO_n] structural units (n = 3, 4) in the vicinity of the [TeO_3] structural units. The increase in the intensity of the band located at about 600 cm^{-1} shows that the formation of the [FeO_4] structural units. It seems that the formation of [TeO_4] structural units is reduced because the modified [TeO_3] units containing one or more Te-O-Pb bonds are unable to accept a fourth oxygen atom.

With the adding of Fe_2O_3 in the host matrix which tend to coordinate with Fe^{+3}, will contribute to coordinate with glass former cation ions. According to the electronegativity theory, the covalency of the bond will become stronger with the decrease of the difference of electronegativity between cation and anion ions. Since the values of electronegativity, for Te, Fe, Pb and O elements are 2.1, 1.83, 2.33 and 3.5, respectively, the covalency of Pb-O are stronger than Te-O and Fe-O, respectively. As a result, the covalency of Te-O and Pb-O bonds is stronger than this of the Fe-O bond.

Accordingly, the excess of non-bridging oxygen ions will coordinated with iron ions only after the tellurium and lead cations attain the maximum of the number of coordination (tellurium atoms – 4 and lead atoms - 4), in agreement with our FTIR data.

iii) For sample with x = 20 mol% Fe_2O_3, the participation of the lead ions than network former yields drastically modifications in the IR spectrum and the change from the lead-tellurate network to the continuous iron-lead-tellurate network with interconnected through Pb-O-Te, Pb-O-Fe and Te-O-Fe bridges. This compositional evolution of the structure could be explained by considering that the excess of oxygen may be accommodated by the conversion of some [FeO_4] to [FeO_6] structural units. A new band appears at 470 cm^{-1} corresponding to the Fe-O vibrations from [FeO_6] structural units [19].

iv) For sample with $x \geq 30$ mol% Fe_2O_3, the increasing trend towards higher wavenumbers of the bands located in the region between 550 and 850 cm^{-1} can be due to the conversion of [TeO_4] into [TeO_3] structural units. A noticeable change appears in content of [TeO_3] structural units.

Iron in the oxidation state +3 is reported to occur predominantly in fourfold coordinations, as $[FeO_4]^{-1}$. These tetrahedral geometries have a negative charge and hence need cations, in the

case of the glasses studied, Pb^{+2} for charge compensation. Accordingly, it is possible a better stabilization of Fe^{+3} from $[FeO_4]^{-1}$ tetrahedral geometry through compensation with Pb^{+2} ions.

The presented observations in these mechanisms show that the lead ions have an affinity pronounced towards $[TeO_3]$ structural units yielding the deformation of the Te-O-Te linkages and pursuant to the intercalation of $[PbO_n]$ (n=3, 4) and $[FeO_n]$ (n=4, 6) entities in the $[TeO_4]$ chain network. The formation of $[FeO_4]^{-1}$ structural units with negative charge implies the attraction of Pb^{+2} ions for charge compensation.

UV-VIS spectroscopy

The iron is present in glasses as Fe^{+2} and Fe^{+3} ions, both of which can exist in tetrahedral and octahedral sites [20-25]. Each redox and coordination state produces its own set of characteristic optical absorption bands. The majority of Fe^{+3} ions are believed to occupy tetrahedral network-forming sites in glasses, although this has been disputed [20-23]. Conversely, the majority of Fe^{+2} ions are through to occupy octahedral network modifying sites [21, 24, 25].

Fe^{+2} produce an oxygen-iron charge transfer band centered in the ultraviolet [26]. Spin-forbidden bands are also expected in the 450-550 nm, but have been ignored in most studies of iron absorption in glasses. Then, Fe^{+2} ions yield two main spin allowed d-d absorption bands located at about 1100 nm and has been attributed to a range of distorted octahedral sites. Accordingly, the energy diagram of the $3d^6$ configuration (Fe^{+2}) indicates that its spectrum will consist essentially of a single band in the infrared region as well as a number of very weak spin-forbidden bands in the visible and ultraviolet regions.

The Fe^{+3} ions produce a more complicated set of absorptions than Fe^{+2}. Since the Fe^{+3} ion has a d^5 configuration, all d-d transitions are forbidden by spin-selection rules [27]. This means they are approximately 10-100 times less intense than spin-allowed transitions. The majority of Fe^{+3} d-d bands are observed at wavelength in the 325-450 nm region, although some Fe^{+3} bands are observed at wavelength as low as 700 nm.

The UV-VIS absorption spectra of $xFe_2O_3 \cdot (100-x)[4TeO_2 \cdot PbO_2]$ glasses with x = 0-60 mol% are shown in Fig. 2. The examinations of these spectra show that the characteristic UV-VIS bands are modified namely:

i) For all glasses, the UV absorption bands begin at 250 nm by an ascending lobe. These UV absorption bands are assumed to originate lead tellurate host matrix. The stronger transitions in the UV-VIS spectrum can be due to the presence of the Te=O bonds from [TeO_3] structural units and Pb=O bonds from [PbO_3] structural units which allow n-π^* transitions. Ions Pb^{+2} with s^2 configuration absorb strongly in the ultraviolet and yield broad emission bands in the ultraviolet and blue spectral area. The intense band obtained centered at about 310 nm corresponds to the Pb^{+2} ions [28].

ii) By introduction of low Fe_2O_3 content ($x \leq 5$ mol%) in the host matrix, the formation of new absorption UV bands is dominant. These bands located in the 320-450 nm region are due to the presence of the Fe^{+3} ions. Then, the intensity of absorption band located at about 250 nm increases and the iron in some cases is reduced to Fe^{+2} by trapping electrons [29]. Some weak bands appear in the 450-550 nm region. These bands show that some Fe^{+3} were converted to Fe^{+2} ions.

Such tendency can be interpreted by the conversion of the Fe^{+3} to Fe^{+2} species and the same time of the present Pb^{+2} ions are oxidized to Pb^{+4} ions. Based on these experimental results, we propose the following possible redox reactions:

$$2\ Fe^{+3} + 2e^- \leftrightarrow 2\ Fe^{+2}$$

$$Pb^{+2} \leftrightarrow Pb^{+4} + 2e^-$$

The increase of intensity of the band situated near 300 nm can be attributed the formation of new Pb=O bonds from [PbO_3] structural units.

iii) The addition of Fe_2O_3 content until 15 mol% causes a decrease in the intensity of the UV absorption bands situated in the 320-450 nm domain. This noticeable decrease can be due the iron ions can participate as former network. The sharp of the increase trend of the IR bands located at about 600 cm^{-1} shows the vibrations of the Fe-O bond from [FeO_4] tetrahedral structural units (Fig. 1).

iv) Further by increasing of Fe_2O_3 content up to 20 mol%, the observed shift of the UV band from 250 to 260 nm and the apparition of new band located at about 285 nm is correlated to the possible distortion of the iron species symmetry. The new IR band situated at about 470 cm^{-1} can be attributed to the [FeO_6] octahedral units. The evolution of the structure can be

explained considering the accommodation of the network with excess of oxygen by the conversion of some [FeO_4] to [FeO_6] structural units.

v) For sample with x=30mol% Fe_2O_3, a new band appears at about 267 nm. This tendency can be explain again to the distortions of the iron species. It is possible a conversion of the [FeO_6] to [FeO_4] structural units. The intensity of the band centered at about 600 cm^{-1} increase in the FTIR spectrum. These inter-conversions of geometry decrease by increasing of Fe_2O_3 content up to 40 mol%.

vi) The very intense transitions appear in the sample with x = 50 mol% Fe_2O_3. New band of larger intensity situated at about 305 nm are due to the presence of Pb^{+2} ions. The bands located in the 250-277 nm region are due to a strong oxygen-iron charge transfer derived to the Fe^{+2} and Fe^{+3} ions. The increase in the intensity of the IR band located at about 689 cm^{-1} shows the vibrations of the Fe^{+2}-O-Fe^{+3} linkages [19]. On the other hand, these intense transitions can be due to formation of [TeO_3] structural units from [TeO_{3+1}] structural units, in agreement with Raman spectra.

vii) For sample with x = 60 mol% Fe_2O_3, the UV absorption bands situated in the 250-290 nm disappear and new bands appear at 320 nm. These bands show the presence of new Fe^{+3} ions. Then, the kink located at about 430 nm is characteristic of Fe^{+3} ions in octahedral symmetry. Also, it is suggested that some of the Fe^{+2} ions present capture positive holes and are converted to Fe^{+3} according to the following photochemical reactions:

$$Fe^{+2} + \text{positive holes} \rightarrow Fe^{+3}$$

$$Pb^{+4} + 2e^{-} \rightarrow Pb^{+2}$$

It seems that some of the Fe^{+2} ions capture positive holes and are transferred to Fe^{+3} ions through photochemical reaction. This mechanism explains the observed increase in the UV region.

The observed continuous increase of the UV band intensity with adding of the Fe_2O_3 content can be related to the progressive growth of induced color centers. This color center is obviously correlated with the transformation of Fe^{+2} to Fe^{+3} ions by capturing positive holes.

In brief, UV-VIS spectroscopic data show two mechanisms: i) the conversion of the Fe^{+3} to Fe^{+2} species in same time with the oxidation of Pb^{+2} to Pb^{+4} ions for sample with smaller Fe_2O_3 content; ii) when the Fe_2O_3 content is higher ($x \geq 50$mol%), the Fe^{+2} ions capture positive holes and are transferred to Fe^{+3} ions through photochemical reaction while the Pb^{+2} ions are formed by reduction of the Pb^{+4} ions.

The conduction in ternary iron oxide glasses was confirmed to be due to hopping conduction of polaron [1, 4-7]. In the conduction of these glasses, a valence change, $Fe^{+2} \rightarrow Fe^{+3} + e^-$ takes place between two iron ions in the glass. The Fe^{+3} ions in excess are sixfold coordinated and the remaining Fe^{+3} ions are in fourfold coordinated. The redox can also control the tetrahedral to octahedral Fe^{+3} ratio: an increase of Fe^{+3} leads to an increase of octahedral Fe^{+3}.

DFT calculations

In the quantum chemical calculations we will use the IR and UV-VIS data in order understand of the local structure $50Fe_2O_3 \cdot 50[4TeO_2 \cdot PbO_2]$. Similar methodology has previously been reported to study other glasses [30-34]. The study on structural modifications of the vitreous network and the equilibrium geometry were found by optimization (Fig. 3).

There are some sites in our model (Fig. 3), namely:

i) The basic coordination polyhedrons are $[TeO_4]$ structural units which can be found in the glass in four states: tetrahedral, square pyramids, trigonal bipyramids, and trigonal bipyramids with three strong bonds and one elongated axial bond. The Te-O bonds from the square pyramids have shorter interatomic distances (2x1.74 and 2x1.85 Å) than the covalent Te-O bond length (2.15 Å). The Te-O bonds from tetrahedral geometry have one bond with shorter interatomic distances (1.78 Å) and three bonds with longer interatomic distances (1.87 Å).

The Te-O bonds of the irregular polyhedrons are subdivided into two groups: (1) three bonds have shorter interatomic distances (1.74-1.82Å) and one has intermediate interatomic distance (1.92-2.02 Å); (2) three bonds have intermediate interatomic distances (1.95-2.05 Å) and one has longer interatomic distances (3.05 Å) but significantly shorter than the sum of the van der Waals radii (3.58 Å). These irregular polyhedrons are situated in the vicinity of the $[PbO_n]$ and $[FeO_n]$ structural units.

Accordingly, the [TeO_4] structural units have a marked tendency towards deformation and lability of one of the axial bonds. This lability is sharply increased in the liquid state, where due to kinetic factors the axial bonds easily undergo a dynamic elongation over 2.15 Å. The coordination number of the tellurium atom changes from 4 to 3+1 and marked tendency towards elongation of the Te-O distances over 2.15 Å is observed. In the last states, as a consequence, a 3+1 coordination of the tellurium atom is required. The extent of bond deformation, besides the kinetic factors, is also influenced by the composition, temperature and viscosity of the melt, by the nature of the modifier, as well as by some thermodynamic factors.

ii) The presence of [TeO_3] polyhedra in the glass is also possible and depends strongly on the modifier concentration. The Te-O distances are divided into three sets: a set of three shorter distances range from 1.79 to 1.85 Å, three have intermediate bonds range from 1.93 to 2.06 Å and one has longer interatomic distance (3.39 Å).

iii) In this structure, four-coordinated lead atoms occupy two different sites. The first are coordinated with four oxygen atoms forming distorted tetrahedral octahedral geometries, the four Pb-O bonds have short interatomic distances (1.98-2.13 Å). The second lead atom has ionic character. One Pb-O bond have shorter interatomic distances (2.11 Å), one has longer Pb-O bond distances (2.83 Å) than the Pb-O covalent bond (2.22 Å) but significantly shorter than the sum of the van der Waals radii (3.54 Å) and two oxygen atoms remain relatively far away from lead cation (4.12-4.75 Å). These bonds are too long to be accepted as a chemical bond in the usual sense.

iv) The three-coordinated lead atoms are in two diverse sites. In the first site, three bonds have shorter interatomic distances (1.90-2.06 Å). Another site has two shorter interatomic distances (2.19-2.21Å) and one Pb-O bond has longer interatomic distance (2.96 Å) than the Pb-O covalent bond.

v) Iron site is coordinated to four oxygens atoms. The three bonds have shorter Fe-O interatomic distances (1.79-1.87 Å) and one has longer interatomic distance (1.93 Å). The EXAFS analysis [35] reveals that in the iron glasses, the Fe-O bond length is equal to 1.86-1.88 Å in the [FeO_4] tetrahedral structural units. The distance of 1.93 Å is intermediate between that corresponding to tetrahedral (1.88 Å) and octahedral (2.00 Å) coordinated iron [36]. Therefore, it is expected that in this sample, the iron atoms occupy both tetrahedral and

octahedral sites. The majority of Fe^{+3} ions are believed to occupy tetrahedral network-forming sites in glasses while the majority of Fe^{+2} ions are through to occupy octahedral network modifying sites. Then, the reduction of Fe^{+3} to Fe^{+2} always acts a network modifier, forms $[FeO_6]$ structural units during glass melting is possible.

Additionally, the EXAFS analysis [35] disclosed that the coordination number of iron depends on the Fe_2O_3 concentration. Accordingly, the number of the oxygen atoms attached in the $[FeO_4]$ structural units decreases when the Fe_2O_3 concentration increases suggest that the tetrahedral coordination of iron into the glass is destroyed.

The distribution of the electronic states of the HOMO and LUMO can be seen in Fig. 4. An interesting finding in these systems is that:

i) The HOMO gives character of electron donor for the $[TeO_4]$ structural units.

ii) The LUMO gives the character of electron acceptor for the $[TeO_3]$ structural units of the network.

iii) The $HOMO^{-1}$ gives character of electron donor for the $[TeO_4]$, $[TeO_3]$ structural units and Fe^{+2} ions.

iv) The $LUMO^{+1}$ gives the character of electron acceptor for the $[TeO_3]$ and $[TeO_4]$ structural units of the network.

There is a change transfer between the tellurium atoms tri- and tetra-coordinated. This can be explained considering that the lead-tellurate network is flexible to form the appropriate coordination environments with structural units of opposite charge such as iron ions, $[FeO_4]^{-1}$.

Accordingly, the addition of Fe_2O_3 content to lead-tellurate glasses seems to break the axial Te-O bonds because of the strong polarizability of the tellurium lone pair electrons and leads to the formation of glass structure. As a result more non-bridging Te-O bonds are formed and the $[TeO_4]$ structural units are transformed little by little into $[TeO_{3+1}]$ and $[TeO_3]$ type polyhedra when the metal oxides are added more and more. The analysis of these data further indicates with an increase in the concentration of Fe_2O_3, a gradual adaptation of lead ions from covalent to ionic environment.

Raman spectroscopy

Fig. 5 shows the Raman spectra of the $xFe_2O_3 \cdot (100-x)[4TeO_2 \cdot PbO_2]$ glasses with x=0-60mol%. The shape of the Raman spectra is influenced by the presence of iron oxide in the studied glasses. The bands centered at around 465cm^{-1} are assigned to the stretching vibrations of Te-O-Te linkages [37]. The bands centered at around 652cm^{-1} are originated from vibration of the continuous networks composed of $[TeO_4]$ tetragonal bipyramids and the bands centered at around 710cm^{-1} are contributed to $[TeO_{3+1}]$ and $[TeO_3]$ structural units [38]. It is found that the maximum phonon energy of doped glasses increased from 710 to 745 cm^{-1} gradually. With the increase of Fe_2O_3 content up to 60moli%, the number of $[TeO_{3+1}]$ coordinated polyhedral and $[TeO_3]$ trigonal pyramidal structural units increase in the network structure.

The $[TeO_{3+1}]$ unit can be thought of as distorted trigonal bipyramidal $[TeO_4]$ units, with one oxygen further away from the central tellurium than the remaining three oxygen. This increase in lower coordination at the expense of higher coordination units is indicative of depolymerization of the lead-tellurite glass network.

The Raman band centered at about 270 cm^{-1} may be associated with Pb-O stretching and O-Pb-O bending vibrations. The strong bands situated near 120 and 135 cm^{-1} in the Raman spectra of iron-lead-tellurate glasses is almost certainly due to Pb-O symmetric stretching vibration [39, 40]. One evidence in support is that the relative intensity of this band increases with the increasing of Fe_2O_3 content of the glasses from x = 1 to 40 mol% Fe_2O_3, after that its intensity decreases evidently. This shows that the high doped with Fe_2O_3 content can cause the broken of Pb-O bond in iron-lead-tellurate glasses. On the other hand, this is need because the content of $[TeO_3]$ structural units increases. For samples with $x \geq 50$ mol%Fe_2O_3, the increases in intensity of the UV-VIS bands located at about 310nm check up this hypothesis.

The fact that this band is very strongly polarized also indicates a high degree of symmetry of the nearest neighbors of lead atoms [39]. Except the drop of the intensity of 135 cm^{-1}, we find no new bands appear in the Raman spectra. By increasing of the higher Fe_2O_3 content, the 135 cm^{-1} band would then be the Pb-O symmetric stretch of $[PbO_4]$ pyramidal units. We think that the higher doped can cause the broken of Pb-O bonds and make the $[PbO_4]$ structural units change to $[PbO_3]$ chains [41]. For sample with x = 60 mol%, supplementary, well-defined

Raman band appears around 415 cm^{-1}. This band is due to the covalent Pb-O bond vibrations [42, 43].

For higher Fe_2O_3 content, the Raman spectra revealed a greater degree of depolymerization of the vitreous network than do the FTIR spectra. It seems that the Raman spectroscopy is a more sensitive technique to the changes that appear in the short-range order of our glass structure at Fe_2O_3 addition.

Conclusions

We were analyzed the effects of iron ions on structure of the lead-tellurate glasses by investigations of FTIR, Raman and UV-VIS spectroscopy. Based our results, we conclude that the accommodation of the networks with the excess of oxygen it is possible by the deformation of Te-O-Te linkages, the participation of lead and iron atoms as former network and the intercalation of $[FeO_6]$ entities in the $[TeO_4]$ chain network.

Our UV-VIS spectroscopic data show the existence of the reversible redox process in the matrix host by increasing of the Fe_2O_3 content. For smaller Fe_2O_3 content the mechanism implies the conversion of the Fe^{+3} to Fe^{+2} species in same time with the oxidation of Pb^{+2} to Pb^{+4} ions. Inversion redox processes take place for higher Fe_2O_3 content.

DFT calculations show that the $[TeO_4]$ structural units have a marked tendency towards deformation and lability of one of the axial bonds. This can be explained considering that the lead-tellurate network is flexible to form the appropriate coordination environments with structural units of opposite charge such as iron ions, $[FeO_4]^{-1}$.

The Raman spectra show that a very strong depolymerization appears in studied iron-lead-tellurate glasses with the Fe_2O_3 addition. The bands due to the Pb-O bond vibrations are very strongly polarized indicating a high degree of symmetry of the nearest neighbors of lead atoms. The intensity of band around 720 cm^{-1} increases relative to the band at 660cm^{-1} with increase in Fe_2O_3 content indicating that the $[TeO_4]$ structural units convert into $[TeO_3]$ units via an intermediate coordination labeled as $[TeO_{3+1}]$ structural units.

Acknowledgments

The financial support of the Ministry of Education and Research of Romania-National University Research Council (CNCSIS, PN II-IDEI 183/2008, contract number 476/2009) is gratefully acknowledged by the authors.

References

1. Dhawan VK, Mansingh A, Sayer M (1982) J Non-Cryst Solids 51:87-103
2. Sega K, Kasai H, Sakata H (1998) Mater Chem Phys 53:28-33
3. Qiu HH, Ito T, Sakata H (1999) Mater Chem Phys 58:243-248
4. Qiu HH, Kudo M, Sakata H (1997) Mater Chem Phys 51:233-238
5. Simon S, Pop R, Simon V, Coldea M, (2003) J Non-Cryst Solids 331:1-10
6. Simon S, Todea M (2006) J Non-Cryst Solids 352:2947-2951
7. Pan A, Ghosh A (2002) J Mater Sci Lett 21:395-396
8. Pisarski W, Goryczka T, Wodecka-Dus B, Plonska M, Pisarska J (2005) Mater Sci Eng B 122:94-99
9. Hoppe U, Yousef E, Rüssel C, Neuefeind J, Hannon AC (2002) Solid State Commun 123:273-278
10. Frisch MJ, Trucks GW, Schlegel HB, Scuseria GE, Robb MA, Cheeseman JR, Montgomery JA Jr, Vreven T, Kudin KN, Burant JC, Millam JM, Iyengar SS, Tomasi J, Barone V, Mennucci B, Cossi M, Scalmani G, Rega N, Petersson GA, Nakatsuji H, Hada M, Ehara M, Toyota K, Fukuda R, Hasegawa J, Ishida M, Nakajima T, Honda Y, Kitao O, Nakai H, Klene M, Li X, Knox JE, Hratchian HP, Cross JB, Adamo C, Jaramillo J, Gomperts R, Stratmann RE, Yazyev O, Austin AJ, Cammi R, Pomelli C, Ochterski JW, Ayala PY, Morokuma K, Voth G A, Salvador P, Dannenberg JJ, Zakrzewski VG, Dapprich S, Daniels AD, Strain MC, Farkas O, Malick DK, Rabuck AD, Raghavachari K, Foresman JB, Ortiz JV, Cui Q, Baboul AG, Clifford S, Cioslowski J, Stefanov BB, Liu G, Liashenko A, Piskorz P, Komaromi I, Martin RL, Fox DJ, Keith T, Al-Laham MA, Peng CY, Nanayakkara A, Challacombe M, Gill PMW, Johnson B, Chen W, Wong MW, Gonzalez C, Pople JA (2003) Gaussian 03, Revision A1. Gaussian Inc, Pittsburgh PA
11. Rada S, Culea M, Culea (2008) J Non-Cryst Solids 354:5491-5495
12. Rada S, Rada M, Culea E (2010) Spectrochim Acta A 75:846-851
13. Rada S, Culea M, Rada M, Culea E (2010) J Alloys Compd 490:270-276
14. Rada S, Neumann M, Culea E (2010) Solid State Ionics 181:1164-1169
15. Mandal S, Hazra S, Ghosh A (1994) J Mater Sci Lett 13:1054-1055
16. Hazra S, Ghosh A (1995) J Mater Res 10:2374-2378
17. Rada S, Culea M, Neumann M, Culea E (2008) Chem Phys Lett 460:196-199
18. Rada S, Ristoiu T, Rada M, Coroiu I, Maties V, Culea E (2010) Mater Res Bull 45: 69-73

19. Zhang Z (1993) Phys Chem Glasses 34:95-103
20. Carnevale, A, Peterson, GE, Kurkjian, CR (1976) J Non-Cryst Solids 22:269-275
21. Montenero A, Friggeri M, Giori D C, Belkhiria N, Pye LD (1986) J Non-Cryst Solids 84:45-60
22. Kurkjian CR (1970) J Non-Cryst Solids 3:157-194
23. Park JW, Chen H (1980) J Non-Cryst Solids 40:515-525
24. Edwards RJ, Paul A, Douglas RW (1972) Phys Chem Glasses 13:137-143
25. Rossano S, Ramos A, Delaye JM, Filipponi A, Creux S, Brouder C, Calas G (1999) J Synchrotron Radiation 6:247-248
26. Edwards RJ, Paul A, Douglas RW (1972) Phys Chem Glasses 13:137-143
27. Burns RG (1993) Mineralogical Applications of Crystal Field Theory, Cambridge University, Cambridge, p 57
28. Ehrt D (2004) J Non-Cryst Solids 34:822-829
29. Friebele EJ (1991) In: Ullmann DR, Kreidl NJ (eds) Optical Properties of Glass. American Ceramic Society, Westerville, Ohio, USA, p 205
30. Rada S, Chelcea R, Culea M, Dehelean A, Culea E (2010) J Mol Struct 977:170-174
31. Rada S, Culea M, Culea E (2008) J Phys Chem A 112:11251-11255
32. Rada S, Culea E (2009) J Mol Struct 929:141-148
33. Rada S, Culea E, Neumann M (2010) J Mol Model 16:1333-1338
34. Rada S, Chelcea R, Culea E (2010) J Mol Model. doi:101007/s00894-010-0706-8
35. Pinakidou F, Katsikini M, Kavouras P, Komninou F, Karakostas T, Paloura EC (2008) J Non-Cryst Solids 354:105-111
36. Lynn JW, Erwin RW, Rhyne JJ, Chen HS (1983) J Magn Magn Mater 31-34:1397-1398
37. Salem SM (2010) J Alloys Compd 503:242-247
38. Upender G, Sathe VG, Mouli VC (2010) Physica B 405:1269-1273
39. Jia H, Chen G, Wang W (2006) Opt Mater 29:445-448
40. Barney ER, Hannon AC, Holland D, Winslow D, Rijal B, Affatigato M, Feller SA (2007) J Non-Cryst Solids 353:1741-1747
41. Imaoka M, Hasegawa H, Yasui I (1986) J Non-Cryst Solids 85:393-412
42. Ciceo-Lucacel R, Marcus C, Timar V, Ardelean I (2007) Solid State Sci 9:850-854
43. Radu A, Baia L, Kiefer W, Simon S (2005) Vibrat Spectrosc 39:127-130

Tables

Table 1 Assignments of Raman and IR bands of of $xFe_2O_3 \cdot (100-x)[4TeO_2 \cdot PbO]$ glasses

Raman band [cm^{-1}]	IR band [cm^{-1}]	Assignment
120, 135	-	Pb-O symmetric stretching vibration
270	-	Pb-O stretching and O-Pb-O bending vibrations
-	400-500	the Fe-O vibrations from [FeO_6] structural units
405	470	Vibrations of Pb-O covalent bond in [PbO_4] structural units
465	475	The stretching vibrations of Te-O-Te linkages
-	570-600	Fe-O bonds in the [FeO_4] structural units
650-670	620-680	Stretching vibrations of [TeO_4] structural units
-	670, 850, 1050	Pb-O bonds vibrations from [PbO_3] and [PbO_4] structural units
720-735	720-780	Stretching vibrations of [TeO_3]/[TeO_{3+1}] structural units

Figure captions

Fig. 1 FTIR spectra of $xFe_2O_3 \cdot (100-x)[4TeO_2 \cdot PbO]$ glasses with $0 \leq x \leq 60$ mol%

Fig. 2 UV-VIS absorption spectra of $xFe_2O_3 \cdot (100-x)[4TeO_2 \cdot PbO]$ glasses in function of iron oxide content

Fig. 3 The optimized structure of the $50Fe_2O_3 \cdot 50[4TeO_2 \cdot PbO]$ glasses was used to perform the DFT computations

Fig. 4 The distribution of the electronic states of the HOMO (E_{HOMO} = -6.03 eV), $HOMO^{-1}$, LUMO (E_{LUMO} = -1.73 eV) and $LUMO^{+1}$ of the proposed model for $50Fe_2O_3 \cdot 50[4TeO_2 \cdot PbO]$ glasses

Fig. 5 Raman spectra of $xFe_2O_3 \cdot (100-x)[4TeO_2 \cdot PbO]$ glasses with $0 \leq x \leq 60$ mol%

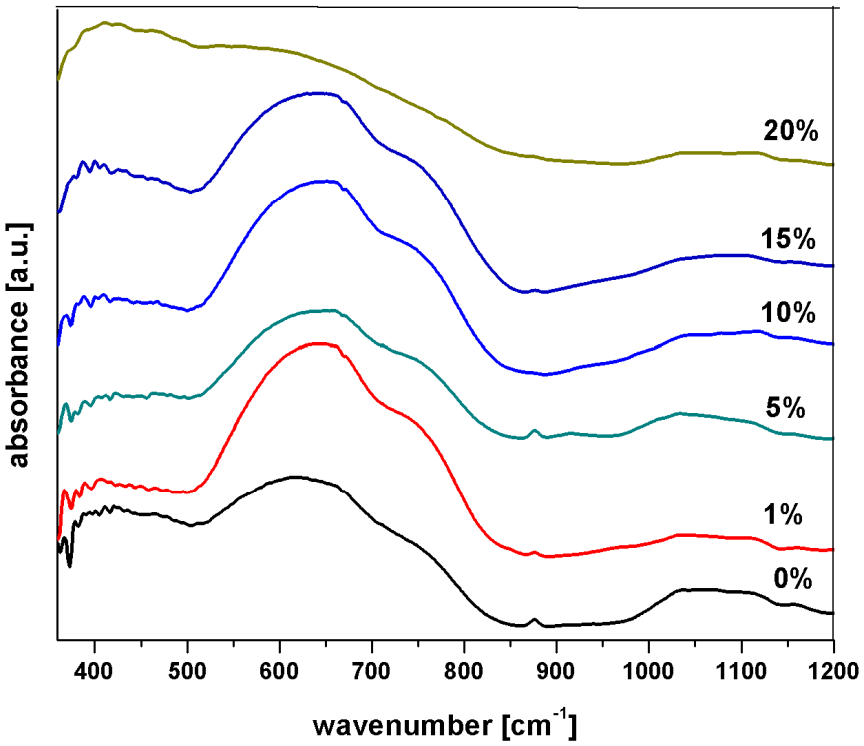
absorbance [a.u.]
wavenumber [cm-1]
20%
15%
10%
5%
1%
0%
400
500
600
700
800
900
1000
1100
1200

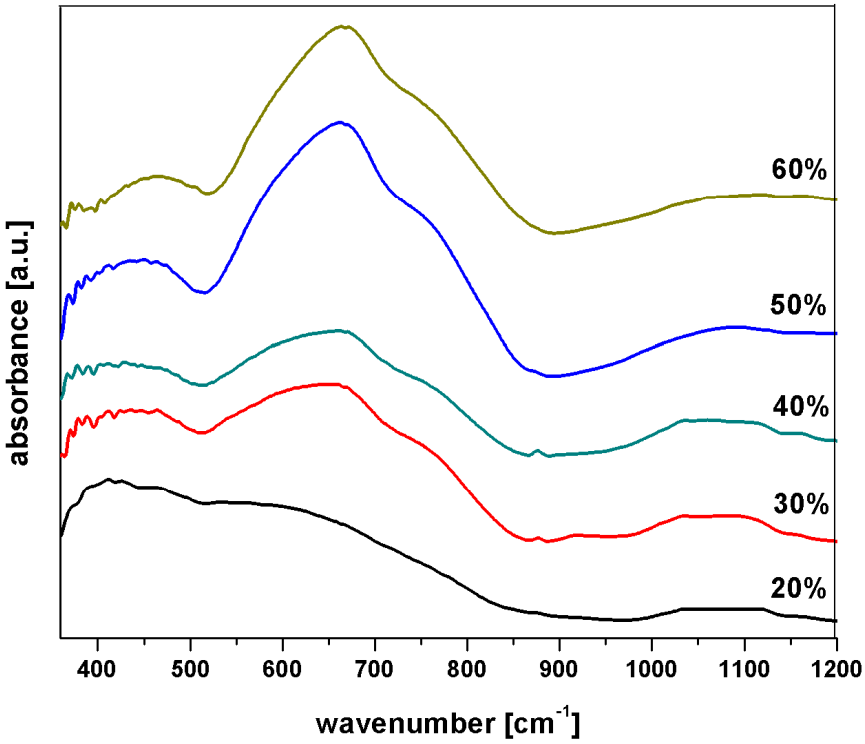
absorbance [a.u.]
60%
50%
40%
30%
20%
400
500
600
700
800
900
1000
1100
1200
wavenumber [cm-1]

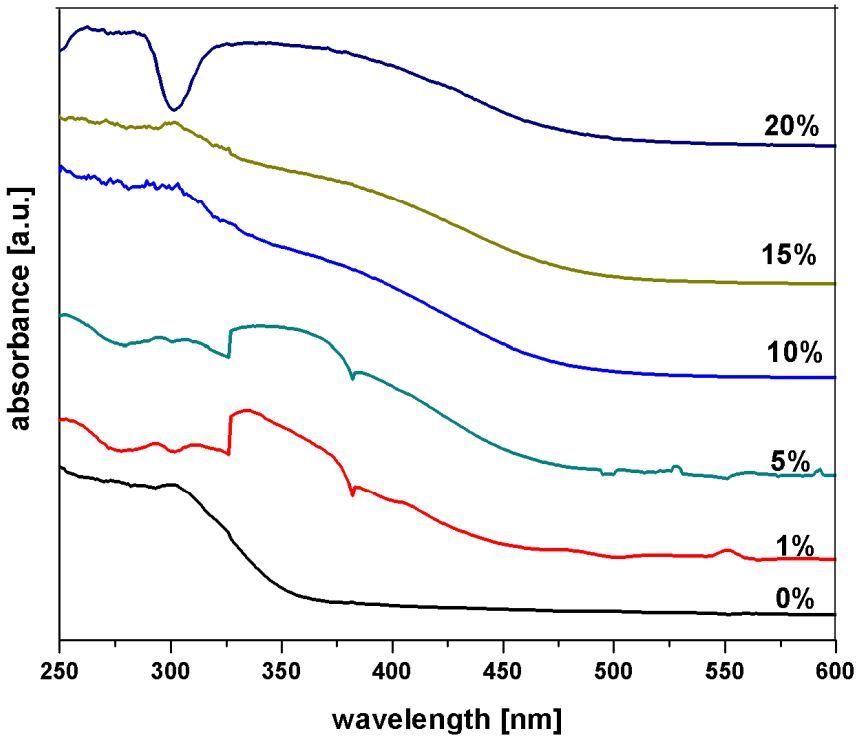
absorbance [a.u.]
wavelength [nm]
250
300
350
400
450
500
550
600
20%
15%
10%
5%
1%
0%

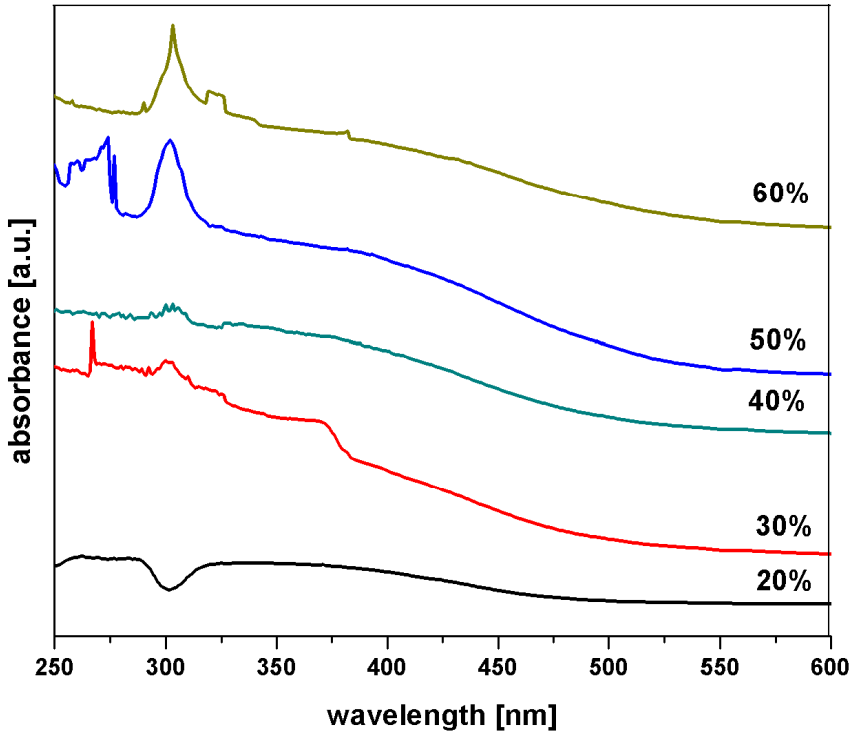
absorbance [a.u.]
60%
50%
40%
30%
20%
250
300
350
400
450
500
550
600
wavelength [nm]

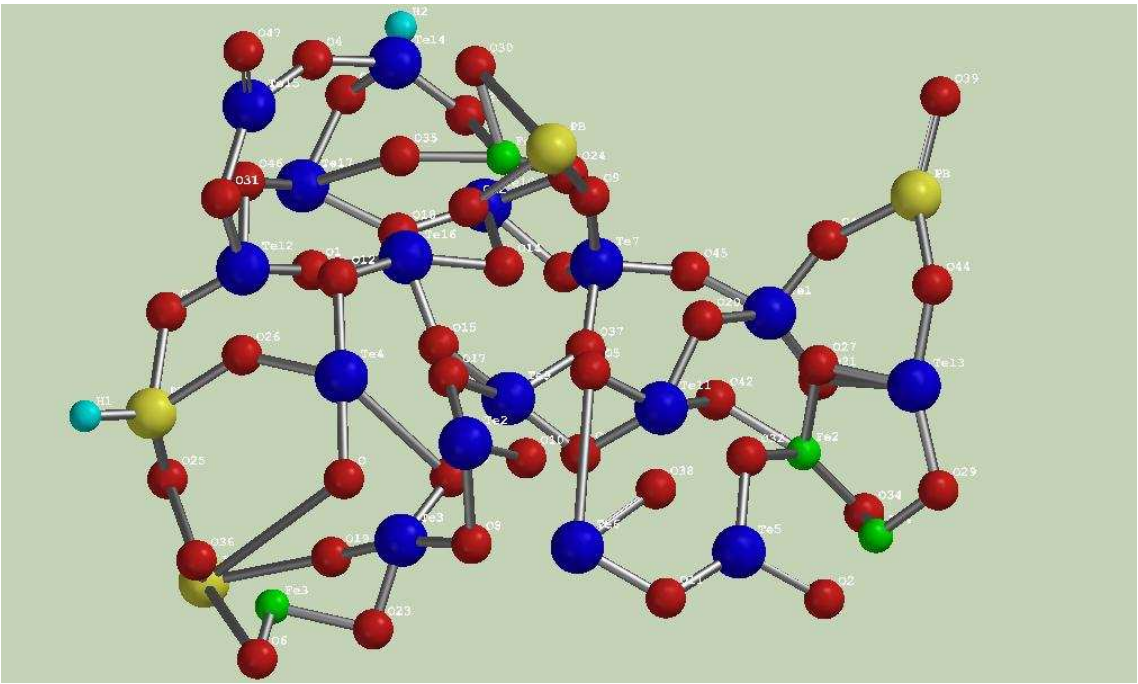

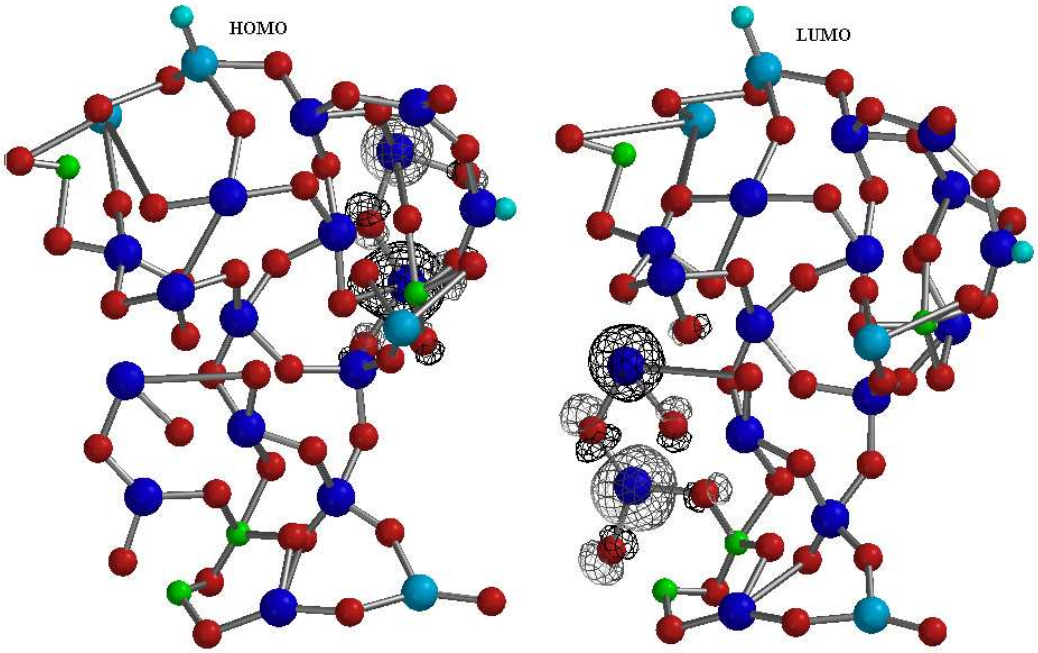
HOMO
LUMO

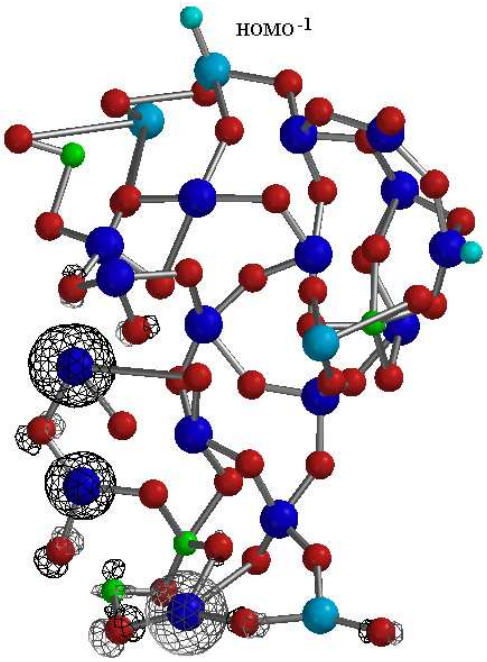
HOMO -1

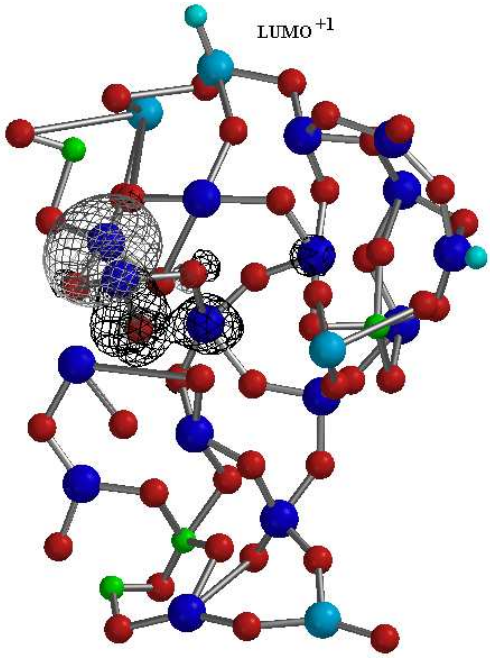
LUMO +1

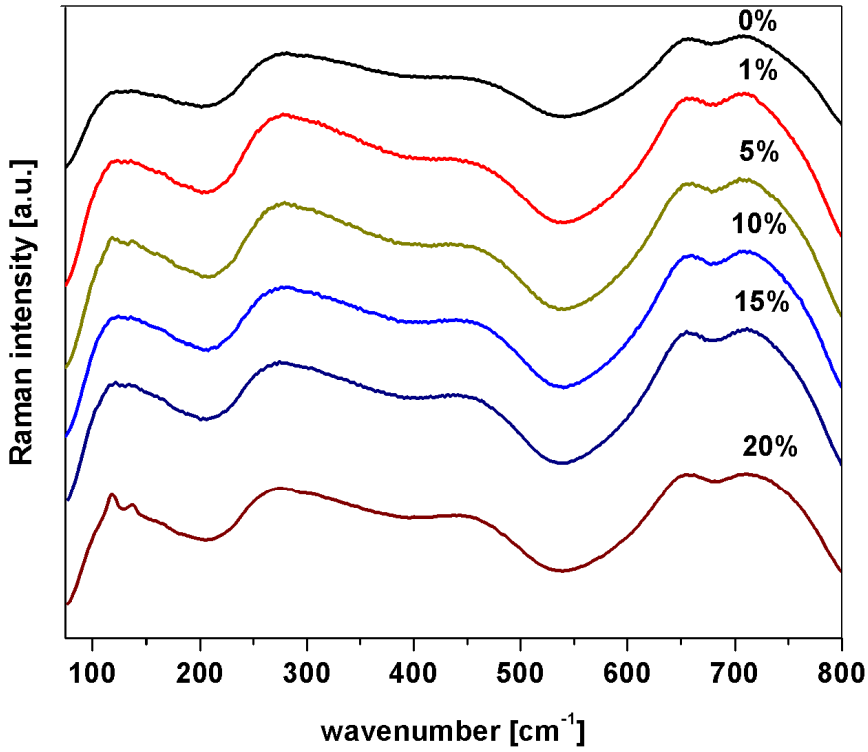
0%
1%
5%
10%
15%
20%
Raman intensity [a.u.]
100
200
300
400
500
600
700
800
wavenumber [cm-1]

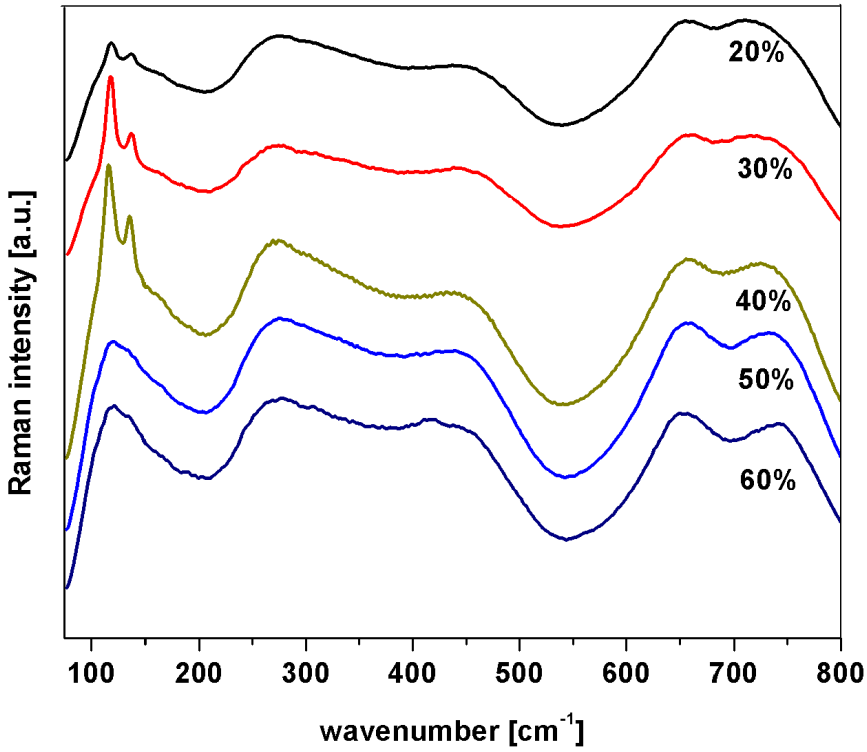
20%
30%
40%
50%
60%
Raman intensity [a.u.]
100
200
300
400
500
600
700
800
wavenumber [cm-1]